ARTICLE TYPE

Assessing the transferability of common *top-down* and *bottom-up* coarse-grained molecular models for molecular mixtures. [†]

Thomas D. Potter,[a] Jos Tasche,[a] and Mark R. Wilson[*a]

The performance of three methods for developing new coarse-grained models for molecular simulation is critically assessed. Two *bottom-up* approaches are employed: iterative Boltzmann inversion (IBI) and the multiscale coarse-graining method (MS-CG), using an atomistic *n*-octane-benzene reference system. Results are compared to a *top-down* coarse-graining approach employing the SAFT-γ Mie equation of state. The performance of each methodology is assessed against the twin criteria of local structure prediction and accurate free energy representation. In addition, the transferability of the generated potentials is compared across state points. We examine the extent to which the IBI methodology can be improved by using a multi-reference approach (MS-IBI), and demonstrate how a pressure correction can be employed to improve the results for the MS-CG approach. Additionally, we look at the effect of including angle-terms in the SAFT-γ Mie model. Finally, we discuss in detail the strengths and weaknesses of each method and suggest possible ways forward for coarse-graining, which may eventually address the problems of structure prediction, thermodynamic consistency and improved transferability within a single model.

1 Introduction

Modern computational chemistry is carried out over many time and length scales, ranging from quantum chemical studies of relatively small systems to atomistic force field-based studies of rather larger systems, to coarse-grained models representing many thousands of molecules.[1,2] As ever, the trade-off between computational cost and accuracy determines the level of theory appropriate for the problem at hand. Over the last few years, considerable progress has been made in improving both the accuracy and speed of models in each of these areas. In addition, progress has been made in linking together models of different resolution at both QM/MM[3,4] and atomistic/coarse-grained levels.[5–8]

Despite recent progress, the area of coarse-grained modelling remains somewhat problematic. Here, two big issues arise: the *representability*[9] and *transferability* problems.[10] The former is concerned with the ability of a coarse-grained model to represent physical properties at the thermodynamic state point at which it is parametrised, the latter is concerned with the ability of the same model to be predictive at different state points, i.e. under conditions where parametrisation data was not available. Both issues are problematic (and often a source of contention) and exist whether or not the coarse-grained model is developed by reference to experimental data (*top-down* coarse-graining)[11,12] or by reference to an underlying atomistic model (*bottom-up* coarse-graining).[13,14]

The problem of representability arises from the fact that a coarse-grained model parametrised to reproduce one observable will not necessarily be able to reproduce other observables of the system at the same state-point.[15,16] Representability is discussed in depth by Wagner *et al.*[9] They emphasise that it is only reasonable for a coarse-grained model to represent observables which are compatible with the resolution of the model, and do not significantly depend on the degrees of freedom which were removed from the all-atom representation. In some cases, the expression for calculating a particular observable in an all-atom representation may not be valid for a coarse-grained representation. For example, the standard virial expression for the pressure is invalid if the coarse-grained potentials are volume-dependent.[9] Some representability issues are subtle. For example, coarse-graining through the elimination of degrees of freedom typically changes the balance of enthalpic and entropic contributions to free energy within a model of a molecular system.[17,18] However, the coarse-grained model might still capture the correct phase behaviour, provided free energy changes are well-represented.

[a] *Department of Chemistry, Durham University, Lower Mountjoy, Stockton Road, Durham, DH1 3LE, United Kingdom.*
[*] *Author for correspondence. E-mail: mark.wilson@durham.ac.uk*

Representability and transferability both have similar origins: the state-dependence of effective pair potentials.[19,20] However, it is noticeable that transferability differs significantly between different types of coarse-grained models and the coarse-grained systems they represent. In the early days of systematic coarse-graining from reference atomistic models, it was noted that approaches such as iterative Boltzmann inversion (IBI)[21] could be used to provide coarse-grained models of homopolymers that were (sometimes) transferable across a range of temperatures and molecular weights.[22–24] However, it is now recognised that for mixtures containing many types of interaction sites, where chemical environment often changes with concentration and/or temperature, transferability (and representability) becomes far more problematic. Also, as polymer melts are usually isotropic, it was initially hoped that simple time-scale scaling could be used to link dynamic properties between atomistic and coarse-grained levels.[13] However, for systems with anisotropy or inhomogeneity, or simply with different activation barriers for different processes, there is no guarantee that different dynamic quantities are not accelerated by different amounts in moving from an atomistic to a coarse-grained model.

From a chemical perspective, two key areas where more accurate (both representative and transferable) coarse-grained models are most needed are in: i) the prediction of local structure and ii) the prediction of free energy changes as a function of changing temperature and/or concentration. The former underpins the use of coarse-grained models to predict complex supramolecular or self-organised structures. This is vital in many areas of biochemical modelling, including prediction of membrane structure and stability[25–27] and protein/nucleic acid interactions.[28] Structure prediction also underpins many important areas of soft matter chemistry, such as micelle formation[29,30] and the formation of the microphase-separated structures seen in lyotropic liquid crystal[18,31–33] and block copolymer phase diagrams.[34–36] An accurate representation of free energy changes (as a function of temperature and/or concentration) underpins the prediction of thermotropic liquid crystal phase diagrams,[37,38] liquid-liquid miscibility and the phase boundaries in many industrially important soft matter systems formed from polymers and/or surfactants. Hence, there is considerable interest in methods that can automatically generate a coarse-grained model (either from a *bottom-up* or *top-down* perspective) and are representative in terms of local structure and free energy changes; and are (in the best cases) sufficiently transferable to be used over a range of temperatures and concentrations.

In the current paper, we consider three methods that can be used to develop new coarse-grained molecular models: IBI, the multiscale coarse-graining method (MS-CG), and coarse-graining via molecular theory (in this case SAFT-γ Mie). The first two of these are *bottom-up* approaches that rely on a reference atomistic model. The third is a *top-down* approach, which relies on the fitting of coarse-grained potentials to experimental data. Each methodology is able to be semi-automated to generate a coarse-grained model by reference to its underlying input data, without requiring a more traditional (and highly time-consuming) trial and error approach.

We test the models on a molecular mixture of benzene and octane: chosen because it forms a miscible mixture across the full composition range, has molecular flexibility (within the octane), has different coarse-grained bead types, and has a distinct local structure represented by differing bead-bead partial radial distribution functions (RDFs). We critically assess the performance of each approach against the twin criteria of local structure prediction and accurate free energy representation; and, in addition, look at how transferable the generated potentials are to different state points. We demonstrate also how the IBI approach can be improved by using a multi-reference approach (MS-IBI), how pressure corrections can be employed to improve the MS-CG approach, and look at the effect of the addition of angle-terms to the SAFT-γ Mie model.

2 Computational details

2.1 Assessing the representability and transferability

Coarse-grained effective pair potentials are generally state-point dependent, and this will affect the expressions for a range of system observables. However, in this paper, we test to what extent coarse-grained models based only on pair potentials are able to achieve transferability. The comparisons made between atomistic and coarse-grained models are all based on calculations using the standard atomistic expressions for the relevant observables; however, we do note that in some cases these comparisons may not be strictly valid when the coarse-grained model is state-point dependent.[39]

2.2 Atomistic simulations

The IBI and MS-CG coarse-graining methods both require a reference atomistic model. For this work we use an all-atom model, employing a modified version of the GAFF[40] force field. The modified force field, GAFF-LCFF, was parametrised by Boyd and Wilson to accurately capture the experimental densities and heats of vaporization of a range of molecules, including medium chain alkanes.[41,42] All simulations were performed using the GROMACS 4.6 package.[43] We used a leap-frog algorithm, with a time step of 2 fs. A Nosé-Hoover[44,45] thermostat was used to keep the temperature constant, at 298 K unless stated otherwise, and a Parrinello-Rahman[46] barostat was used to keep the pressure constant at 1 bar for const-NpT simulations. A Particle Mesh Ewald[47] (PME) was used to calculate electrostatic interactions, employing a short-range cutoff of 1.2 nm. A 1.2 nm cut-off was used for Lennard-Jones interactions, and a long-range dispersion correction was applied. All bonds were constrained using the Linear Constraints Solver[48] (LINCS) algorithm within GROMACS.

A series of binary mixtures of octane and benzene were simulated with octane mole fractions (x_{oct}) of 0.0, 0.2, 0.3, 0.5, 0.7, 0.8 and 1.0. For each system, a total of 1600 molecules was simulated. Initially, for each system, a short const-NVT equilibration run was carried out, followed by equilibration at const-NpT to allow the density to reach equilibrium. The reference data for coarse-graining was then obtained from a 2 ns production run at const-NpT, at 298 K and 1 bar.

2.3 Parametrisation of *bottom-up* models

2.3.1 Coarse-grained mapping

Coarse-grained mapping was carried out by assigning two heavy atoms and their associated hydrogens to a coarse-grained bead, and setting the interaction site for that bead as the centre of mass of those atoms.

$$\mathbf{R}_I = \sum_i^n \frac{\mathbf{r}_i m_i}{\sum_i^n m_i}, \tag{1}$$

where $\mathbf{R}_I$ is the positions of coarse-grained bead I, $\mathbf{r}_i$ is the position of an atom i which is included in the coarse-grained bead, m_i is the mass of atom i and n is the number of atoms which are mapped to the bead I.

The coarse-grained mapping schemes used are shown in Figure 1. For octane, a 4-site representation was used, with an outer bead type (A) and an inner bead type (B). This gives rise to 3 bonds, 2 angles and 1 dihedral. For benzene, a 3-site representation, with only one bead type (R) and three bonds, was used. This gives rise to a number of nonbonded interactions to parametrise: 3 for pure octane (A-A, A-B and B-B), 1 for pure benzene (R-R), and 2 additional cross interactions (A-R and B-R) for the octane/benzene mixtures. It should be noted that for our bottom-up models, this CG representation does not include intramolecular 1-3 or 1-4 nonbonded interactions.
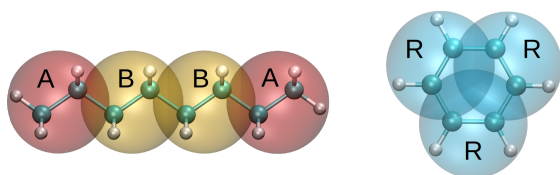

Fig. 1 Coarse-grained mapping scheme for octane and benzene. Each coarse-grained bead represents two carbon atoms and their associated hydrogens.

2.3.2 Iterative Boltzmann inversion (IBI)

IBI (and MS-CG) coarse graining was carried out using the VOTCA-CSG package, versions 1.2.4[49,50] and 1.3.[51] Multi-reference IBI (MS-IBI) was carried out using a modified version of VOTCA 1.3 (as discussed below). Specific values for the parameters used during the fitting are given in the ESI.

Bonded potentials, $U(q)$, were obtained from the equilibrated reference atomistic simulations by simple Boltzmann inversion

$$U(q) = -k_B T \ln P(q), \tag{2}$$

where q is a particular coarse-grained degree of freedom (e.g. a distance, angle or dihedral) and $P(q)$ is the normalised probability distribution of q. Final potentials were extrapolated into poorly sampled regions. For these simple systems, the assumption that bonded interactions are not correlated with other interactions is a good one. As bond stretching potentials for the coarse-grained benzene were very steep (see Supporting Information), the LINCS algorithm was used instead to constrain bonds for that molecule, with the bond length taken as the minimum of

the Boltzmann inverted potential at 0.2203 nm. The bonded interactions parametrised from pure octane and benzene were used in coarse-grained simulations for all concentrations. Bonded potentials and distributions are included in the Supporting Information.

For the (softer) nonbonded potentials, where multi-body effects are important, the potentials from Boltzmann inversion are unable to reproduce the structure of the reference system. For these interactions, an iterative Boltzmann inversion method was required.[52] Here, for each system, separate reference RDFs were calculated for each nonbonded interaction. The RDFs for pure octane and benzene were calculated from trajectories containing 1000 snapshots. For the mixtures, it was found that 5000 snapshots were required for a smooth RDF, due to the decreased sampling of each interaction. These RDFs were used as targets for the IBI procedure.

At each stage of IBI, a coarse-grained simulation was run using a set of test potentials. The first stage used potentials from direct Boltzmann inversion. After each simulation, an update was applied to one of the potentials, according to Equation 3, with each interaction being updated in turn

$$U_{n+1}(r) = U_n(r) + \alpha k_B T \ln \frac{g_n(r)}{g_{target}(r)}, \tag{3}$$

where r is the inter-site distance, $g(r)$ is the radial distribution function and α is a scaling factor on the potential update, which is chosen so that the scheme converges. This procedure was carried out iteratively until the reference and test system RDFs matched to an acceptable degree. Once each interaction had been updated another simulation was run, and a linear pressure correction was applied to all of the potentials simultaneously

$$\Delta U(r) = A\left(1 - \frac{r}{r_{cut}}\right), \tag{4}$$

where

$$A = \mathrm{sgn}(\Delta P) 0.1 k_B T \min(1, |f\Delta P|). \tag{5}$$

In these expressions, r_{cut} is the cut-off distance for the interaction, ΔP is the difference in pressure between the reference and the coarse-grained system and f is a scaling factor, which is chosen to prevent the pressure from oscillating around the desired value. Since the magnitude of the pressure correction depends on ΔP, the correction can be iteratively applied until the pressure of a coarse-grained system is correct.[49,52]

This procedure was repeated until the coarse-grained and target RDFs matched, and the pressure of the system was close to 1 bar. For the 70% and 80% octane systems, the R-R (benzene-benzene) interaction was very difficult to converge compared to the other interactions. For these systems, the procedure was adapted to allow several steps in which only the R-R potential was updated, with care taken to ensure that the other interactions and pressure remained converged.

2.3.3 Multistate IBI (MS-IBI)

MS-IBI was proposed by Moore *et al.*[53,54] to improve transferability of IBI potentials. The idea behind MS-IBI is to use multiple

reference simulations to parametrise a single CG model, allowing a model to be transferable between the state points used for the reference simulations. In the current work, two multi-state IBI (MS-IBI) models were created to test concentration transferability. Each of these models used pure benzene and pure octane as reference systems for the like-like nonbonded interactions, and in addition, simultaneously fitted like-like and unlike interactions with data obtained for mixtures. Model MS-3c, used a mixture of octane and benzene, with $x_{\mathrm{oct}} = 0.5$; and Model MS-4c used two mixtures, with $x_{\mathrm{oct}} = 0.3$ and $x_{\mathrm{oct}} = 0.7$, in addition to the pure octane and pure benzene data. The temperature transferability of MS-IBI models was also tested by constructing models using two reference systems of pure octane at 238 K and 378 K. This model is referred to as MS-2t.

For the MS-IBI fitting, initial guesses for nonbonded potentials were obtained by taking the mean of the Boltzmann inverted potentials of the reference systems included in the fits. At each MS-IBI step, a single potential was updated using Equation 6, with each potential being updated in turn

$$\Delta U(r) = \frac{1}{N} \sum_{i=1}^{N} \eta_i \Delta U_i(r).$$ (6)

Here, N is the number of reference systems, and η_i is a scaling factor chosen to reflect the relative importance of each reference system i. Once the RDFs had converged as much as possible, further iterations were carried out, in which only pressure correction was applied. Here, $\Delta U(r)$ was again calculated using Equation 6, where in this case, $\Delta U_i(r)$ is the linear pressure correction for reference system i.

2.3.4 Multiscale coarse-graining method (MS-CG): force matching of nonbonded interactions

In the MS-CG method, developed by Izvekov and Voth[55] coarse-grained potentials can be constructed by attempting to match the forces acting between CG beads with those from an atomistic reference system that has been mapped onto the CG representation. The method has subsequently been refined and given a strong theoretical basis.[56–58] It is based on a variational principle (see Equation 7), which states that, by minimising the objective function (χ^2), which is related to the difference between the potentials of mean force (PMFs) of the reference and CG systems, one approaches the true effective PMF for the system.[55] The variational principle was rigorously derived from statistical thermodynamics by Noid $et\ al.$.[57]

$$\chi^2 = \frac{1}{3LN} \sum_{l=1}^{L} \sum_{i=1}^{N} |\mathbf{F}_{il}^{\mathrm{ref}} - \mathbf{F}_{il}^{p}(g_1,...,g_M)|^2,$$ (7)

where $\mathbf{F}_{il}^{p}$ and $\mathbf{F}_{il}^{\mathrm{ref}}$ are the total force on bead i in snapshot l, for the coarse-grained and reference systems, respectively, and $g_1,...,g_M$ are coefficients of the function(s) to which the coarse-grained forces are fitted.

The objective of force matching is to minimise χ^2. However, in practice, force matching can be done by solving a series of linear equations in a least-squares manner:[49]

$$\mathbf{F}_{il}^{p}(g_1,...,g_M) = \mathbf{F}_{il}^{\mathrm{ref}},\ i = 1,...,N,\ l = 1,...,L.$$ (8)

The coarse-grained force function is constructed from a series of spline functions, the coefficients of which are obtained by solving Equation 8, with the additional constraint that the first derivatives of the spline functions are continuous. Since the procedure involves matching the total forces in the system, it is vital to select a set of coarse-grained interactions that fully describe the interactions in the system.[49,55]

In the current work, we have implemented the Hybrid Force Matching (HFM) scheme, which allows the combination of two different coarse-graining methods for one system. In this case, the bonded potentials are obtained, as above, through Boltzmann inversion, while the nonbonded potentials are obtained through force matching.[50,59] The use of easily obtainable intramolecular potential functions guarantees sensible molecular geometries and helps eliminate some of the problems that can be associated with a lack of sampling of higher energy conformations in the atomistic reference system. The latter can cause problems if the coarse-grained model is able to sample areas of phase space that the atomistic model does not.[49,60] A number of studies using this hybrid approach have found that is able to give good structural accuracy when applied to a range of soft matter systems.[50,61,62]

The reference non-bonded forces, excluding all intramolecular interactions, were calculated by passing through the reference trajectory and outputting only the forces resulting from intermolecular interactions. The trajectories obtained contained 1000 snapshots; force matching was carried out on blocks of 25 frames each, and the coarse-grained force functions were obtained by averaging over all of the blocks. The resulting force functions were integrated and extrapolated to low inter-site distances to give the HFM coarse-grained potentials for that system.

While our reference simulation were carried out in the const-NpT ensemble, it should be noted that, strictly speaking, the MS-CG method is only valid at constant NVT. A version of the method consistent with the const-NpT ensemble, which includes a volume dependent part, was suggested by Das and Andersen.[63] This was later extended to a volume matching method, which can act as a pressure correction.[64,65] However, this requires including an additional terms (volume) in the pair potential. To avoid these additional terms, we applied a pressure correction to the force-matched potentials using the iterative ramp correction described in Equation 4 (noting that this does not strictly address the state-point dependence). This was applied to each system to give a pressure of close to 1 bar at the experimental density of the system. At each iteration of the pressure correction, a 250 ps simulation was run, and the pressure of the system was calculated based on the final 200 ps of the trajectory. Each of the non-bonded potentials was updated at each iteration, with a small scaling factor to ensure that the pressure converged.

2.4 Parametrisation of *top-down* models

2.4.1 SAFT calculations

The *top-down* method used in this work is based on the Statistical Associating Fluid Theory (SAFT), which is an equation of state forming an algebraic link between macroscopic thermodynamic properties such as densities and free energies, and a molecular bead model. As SAFT can return macroscopic properties within milliseconds, this algebraic link potentially allows a fast parametrisation of CG models from many experimental state points at the same time. Some of the recent extensions to SAFT are based on molecular models with smooth interaction potential functions. This provides the possibility of automatically capturing accurate thermodynamic data within the parametrisation process of a coarse-grained model that is suitable for MD.[66]

SAFT is a perturbation approach, and the SAFT equations are typically expressed in terms of Helmholtz free energies A. As no associating interactions such as hydrogen bonding are expected in this work, we used the non-associating form of SAFT-γ Mie[67]

$$A^{\text{SAFT}} = A^{\text{ideal}} + A^{\text{monomer}} + A^{\text{chain}}, \tag{9}$$

where A^{ideal} accounts for the ideal kinetic and translational energy contributions, A^{monomer} for the change in free energy due to attractive and repulsive interactions between CG beads and A^{chain} for the free energy contribution from forming chains. The monomer contribution term makes use of the Barker–Henderson high temperature perturbation expansion.[68] Perturbation contributions accounting for attractive interactions of up to 3rd order are added to a purely-repulsive hard-sphere reference description $A^{\text{hard-sphere}}$,

$$A^{\text{monomer}} = RTA^{\text{hard-sphere}} + (RT)^2 A_1 + (RT)^3 A_2 + (RT)^4 A_3. \tag{10}$$

The chain contribution term A^{chain} originates from Wertheim's first order thermodynamic perturbation theory.[69–74] The chain forming polymerisation is described as infinitely strong association, which has the same basis as the description of (weaker) association interactions used to capture hydrogen bonding effects (not applied in this work). The free energy change due to the formation of chains is a function of the number of beads per chain m_s and the magnitude of the pair correlation function for the bond length distance $g(\sigma)$,

$$A^{\text{chain}} = -RT(m_s - 1)\ln(g(\sigma)). \tag{11}$$

Using SAFT, predictions can be made for any homogeneous bulk property that can be expressed in terms of Helmholtz free energies, temperature, volume and number of particles. Examples are density, pressure, enthalpy, entropy, Gibbs free energies, heat capacity, thermal expansion and compressibility. Such properties are accessible for both pure components and mixtures, also allowing one to obtain quantities such as free energies of mixing. For example, for a given pressure p_0, the volume V_0 can be optimised to satisfy $-\partial A/\partial V|_{V_0} = p_0$.

Within the SAFT-γ Mie equation of state (EoS), a molecule is represented by a chain of tangentially connected beads interacting with the Mie potential U_{ij}^{Mie}

$$U^{\text{Mie}} = C\varepsilon \left[\left(\frac{\sigma}{r} \right)^{\lambda_r} - \left(\frac{\sigma}{r} \right)^{\lambda_a} \right], \tag{12}$$

with

$$C = \frac{\lambda_r}{\lambda_r - \lambda_a} \left(\frac{\lambda_r}{\lambda_a} \right)^{\frac{\lambda_a}{\lambda_r - \lambda_a}}, \tag{13}$$

where ε and σ are the well depth and the segment diameter, respectively. λ_r and λ_a are the repulsive and attractive exponents, for which $\lambda_r = 12$ and $\lambda_a = 6$ is the usual Lennard–Jones potential. Fitting of the parameters, ε, σ, λ_a and λ_r to reproduce the available experimental data (which could include temperature and concentration-dependent data) leads directly to a coarse-grained molecular model.[75,76]

The Mie parameters for the cross-interactions can be obtained from the following mixing rules:

$$\sigma_{ij} = \frac{\sigma_{ii} + \sigma_{jj}}{2}, \tag{14}$$

$$\lambda_{ij} - 3 = \sqrt{(\lambda_{ii} - 3)(\lambda_{jj} - 3)}, \tag{15}$$

$$\varepsilon_{ij} = (1 - k_{ij}) \frac{\sqrt{\sigma_{ii}^3 \sigma_{jj}^3}}{\sigma_{ij}^3} \sqrt{\varepsilon_{ii}\varepsilon_{jj}}. \tag{16}$$

The k_{ij} parameter allows the well-depth of the cross-interaction, ε_{ij}, to be adjusted (if necessary) to fit experimental mixture data.

SAFT-γ Mie includes no parameters for the intramolecular interactions apart from the Mie potential for non-bonded interactions and σ as a bond length. Therefore chains are effectively modelled as *semi-flexible* without angle or dihedrals interactions but including 1-3 and 1-4 nonbonded interactions. However, in this work, we also investigated the effect of introducing angle potentials to the coarse-grained models produced by the SAFT-γ Mie EoS.

The SAFT calculations were performed with our own implementation of the SAFT-γ Mie expressions, based on the recent publication by Papaioannou *et al.*[77] The SAFT-γ Mie model used the same mapping as the *bottom-up* models, with the one exception that the same interaction potentials were used for beads A and B. The Mie potential parameters of the benzene model were taken from Lafitte *et al.*,[78] who parametrised the Mie potential parameters to match the vapour pressure and liquid density of benzene over a range of temperatures (300–562 K). For octane, Mie potentials were developed using the corresponding state correlation by Mejia *et al.*,[79] in which Mie potential parameters are determined from just three experimental data points: the acentric factor, the critical temperature and the liquid density. The cross-interaction parameters were calculated using Equations 14-16, with $k_{ij} = 0$. The Mie potential parameters are given in Table 1. The interaction potentials were cut at short distances (around 0.5σ, where the value of U_{Mie} is at least $10000 \times kT$) and extrapolated quadratically to lower distances using the same procedure used for bottom-up potentials. This results in a slightly softer interaction potential than a *pure* Mie potential, which is help-

ful when carrying out free energy calculations. Because SAFT is based on tangentially bonded spheres, bond lengths were constrained at σ for MD simulations models.

Table 1 Mie potential parameters obtained for benzene and n-octane

Interaction	σ/nm	ε/K	λ_r	λ_a
R-R	0.3490	258.28	11.58	6.0
A/B-A/B	0.3768	255.92	12.70	6.0
A/B-R	0.3629	256.53	12.13	6.0

2.5 Coarse-grained simulations

The equations of motion were integrated using the leap-frog algorithm of GROMACS with a time step of 2 fs. A Nosé-Hoover thermostat was used to keep the temperature constant at 298 K, and, for constant pressure simulations, a Parrinello-Rahman barostat was used to keep the pressure constant at 1 bar.

For *bottom-up* models, a 1.5 nm cut-off was used for non-bonded interactions. We note that the parametrisation of the non-bonded interactions guarantees a potential which goes to 0 at the cut-off. For each coarse-grained model, a 1 ns constant-NpT production run was carried out, with coordinates output every 0.2 ps. At temperatures other than 298 K, a 500 ps constant-NpT equilibration run was carried out before the production run. Starting structures were obtained from atomistic snapshots, after implementing the mapping shown in figure 1.

For the SAFT-γ Mie model, a 2.0 nm cut-off was used, and all CG bonds were constrained using LINCS. Since the molecular geometry (tangentially bonded spheres) in these models is slightly different to the atomistic structure mapped onto a CG representation, starting structures were constructed by randomly placing 1600 molecules into a box, carrying out a steepest-descent energy minimisation and a 200 ps equilibration run. Production runs were then carried out as for the *bottom-up* models.

2.6 Free energy calculations

We used the Bennett acceptance ratio (BAR) method, which is a commonly used method for calculating the free energy difference (ΔF_{BA}) between two states. For each state, A and B, a separate simulation is run. At regular intervals in the simulation, the Hamiltonian, H, is calculated separately using the force fields for states A and B, and the difference between these two values is determined. The value of a constant, C, for which $\langle f(H_A - H_B + C) \rangle_B = \langle f(H_B - H_A - C) \rangle_A$ is then calculated numerically, which gives an estimate of the free energy difference between A and B,[80]

$$\Delta F_{BA} = RT \ln \frac{\langle f(H_A - H_B + C) \rangle_B}{\langle f(H_B - H_A - C) \rangle_A} + C, \tag{17}$$

where

$$f(x) = \frac{1}{1 + e^x} \tag{18}$$

The free energy estimate is only accurate if there is sufficient overlap between the energy distributions of the two states. Therefore, for most real cases, it is necessary to consider a series of alchemical states between A and B, so that each neighbouring

state has a large energy overlap. The total free energy difference is then calculated as the sum of all the intermediate free energy differences

$$\Delta F_{BA} = \sum_{i=1}^{n-1} \Delta F_{i+1,i} \tag{19}$$

Linear decoupling of van der Waals interactions can result in singularities close to the end points of the decoupling. When the interaction is almost fully decoupled, U will be close to zero at all distances except very close to $r = 0$, where U jumps to a high value. This can be solved by using soft-core potentials for the intermediate states

$$U_{sc}(r) = (1 - \lambda)U_A(r_A) + \lambda U_B(r_B) \tag{20}$$

$$r_A = \left(\alpha \sigma_A^6 \lambda^p + r^6 \right)^{\frac{1}{6}} \tag{21}$$

$$r_B = \left(\alpha \sigma_B^6 (1 - \lambda)^p + r^6 \right)^{\frac{1}{6}} \tag{22}$$

where λ is the coupling parameter, α is the soft-core parameter and p is a positive integer, with α and p chosen to be 0.5 and 1, respectively.

Free energies of solvation were calculated by decoupling the intermolecular interactions of one molecule of octane or benzene with the surrounding solvent, while leaving all intramolecular interactions intact; the solvation free energy is the negative value of the free energy calculated from the decoupling process. All simulations using atomistic and pressure corrected coarse-grained models were run in the const-NpT ensemble, so the energies calculated are Gibbs free energies. Simulations of coarse-grained models without pressure correction were run in the const-NVT ensemble, at the equilibrium density of the atomistic system; the energies from these systems are therefore Helmholtz free energies.

For atomistic systems, Coulombic interactions were decoupled linearly, then van der Waals interactions were decoupled using soft-core potentials with $\alpha = 0.5$ and $p = 1$. Nineteen intermediate λ values were chosen between 0 and 1, with a λ spacing of 0.05.

For coarse-grained systems, van der Waals interactions were decoupled linearly. Between $\lambda = 0$ and $\lambda = 0.9$, a λ spacing of 0.05 was used. In order to prevent singularities just as the interactions were about to disappear, a much higher concentration of λ points was used for $\lambda > 0.9$: typically a spacing of 0.01 up to $\lambda = 0.99$, 0.002 up to $\lambda = 0.998$ and then progressively smaller spacings down to 0.0001 between $\lambda = 0.9999$ and $\lambda = 1.0$. Errors were calculated for each λ spacing to check where additional λ points were required.

Free energies of mixing were also calculated as a further comparison between the atomistic and coarse-grained models. Computational details and results are included in the Supporting Information.

3 Results

3.1 Potentials

The intra- and intermolecular potentials obtained from IBI, HFM and MS-IBI are given in the ESI. Mie potential parameters used in the SAFT-γ Mie model simulations are given in Table 1.
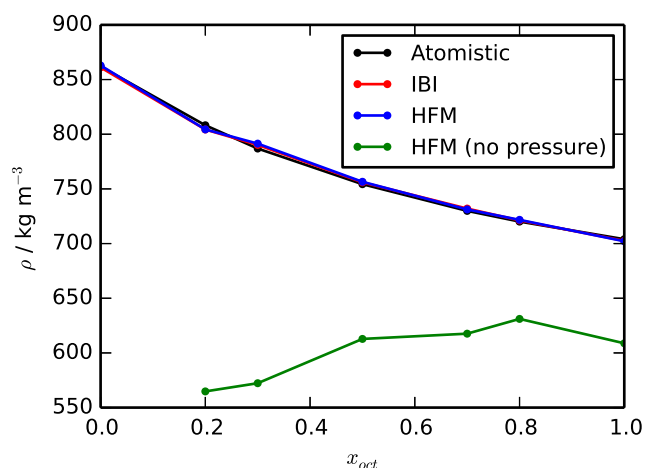
Fig. 2 Comparison of densities calculated using atomistic and coarse-grained simulation models. The IBI and HFM models were parametrised and run at the specified concentration, 298 K and 1 bar. The green line shows results from HFM potentials derived without the benefit of a pressure correction term.

3.2 Densities of single-state models

With a pressure correction applied, the density of each atomistic reference system was reproduced well by both *bottom-up* coarse-grained models parametrised for that concentration, with errors of less than 0.6%, as shown in Figure 2. The accuracy is highly dependent on applications of the pressure correction. Without pressure correction, constant-NVT simulations of the IBI and HFM models at the correct density give pressures of up to 2000 bar, leading to significant errors in density if the same potentials are run at constant-NpT. After the application of pressure correction, all of the models gave pressures of 1 ± 3 bar. Within a force matching methodology, it is usually accepted that the pressure will not be predicted correctly and that these simulations should be run at constant volume, although pressure correction based on a volume-dependent term has been proposed. [63,64] However, Figure 2 shows that a simple linear pressure correction can successfully be applied to force matched potentials within the hybrid scheme employed here.

3.3 Densities from the SAFT-γ Mie model

The densities obtained from molecular dynamics simulations using the potentials developed via SAFT-γ Mie are shown in Figure 3. The results are good with respect to transferability across concentration and temperature ranges, and are indicative of the accuracy of SAFT-γ Mie model as a theory. Here the good quality predictions across changing concentrations rely on the reliability of mixing rules and the corresponding state correlation of Mejia *et al.* [79] We note that SAFT is very versatile in terms of the nature of experimental data that can be fitted and so could be directly fitted to experimental densities to reproduce density data for mixtures. However, these data will not generally be available for many practical coarse-graining applications.
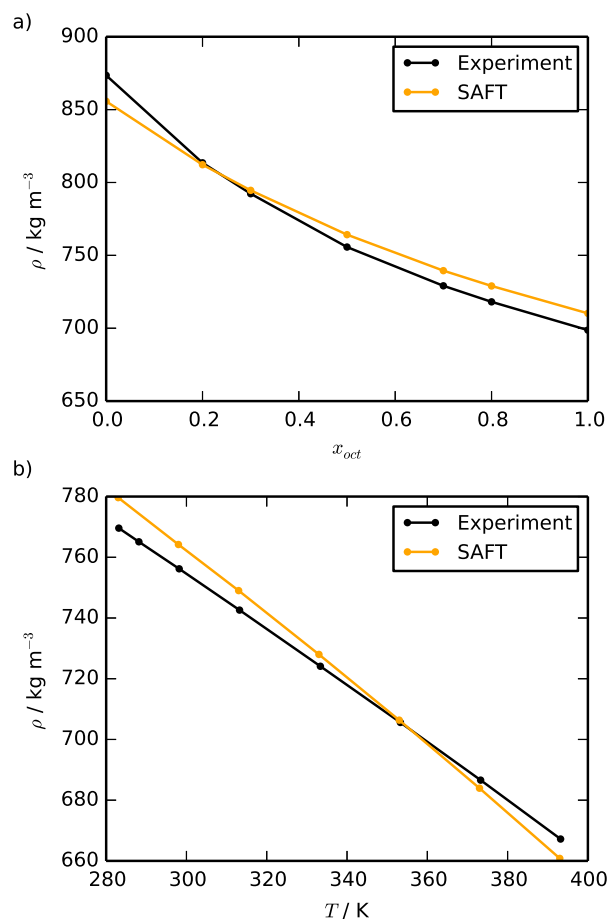

Fig. 3 a) Concentration dependence of mixture densities at 1 bar and 298 K, b) temperature dependence of density at $x_{\text{oct}} = 0.5$ and 1 bar. Results obtained from simulations of SAFT-γ Mie derived potentials and experiment. [81,82]

3.4 Structural accuracy of *bottom-up* and *top-down* models

Figure 4 gives site-site radial distribution functions for the $x_{\text{oct}} = 0.3$ octane system. Unsurprisingly, given the RDF fitting procedure used, the models created using IBI were able to match the radial distribution functions (RDFs) of the atomistic references almost exactly. Although not as good as IBI, HFM is also able to reproduce atomistic RDFs with good accuracy. Similar levels of accuracy have been seen for many systems using full force matching [55,56] (where the bonded interactions are also determined using force matching), and for pure liquid hexane using HFM. [50] However, the results for octane/benzene mixtures confirm that the separation of bonded and non-bonded terms, which is the basis of HFM is also valid for multicomponent systems with a greater number of interactions.

Interestingly, the use of a pressure correction did not significantly affect the RDFs in either the pure components or the mixtures. The linear pressure correction has the greatest effect on the long-range tail of the potential, which has significant effects on thermodynamic properties such as pressure. While the absolute value of ΔU is larger at smaller r (see Equation 4), the attractive well and short-range repulsion are still preserved by the pressure

correction, indicating that these are most important parts of the potential for determining the local molecular packing in the system.

The SAFT-γ Mie RDFs are particularly poor, with high first and second peaks of the RDFs appearing at distances that are too short. The more complex peak shapes present in the atomistic and *bottom-up* coarse-grained RDFs are also absent in the SAFT-γ Mie RDFs. Here, the constraint of using tangential spheres leads to a very different local site-site packing behaviour to the case where neighbouring coarse-grained sites in a molecule are overlapped. This has been noted in recent work which attempted to develop coarse-grained models for a chromonic liquid crystal.[17] In the chromonic study, the tangential constraint directly gave rise to unphysical molecular stacking, which in turn can promote phase separation within a simulation. Such effects are less important at higher levels of coarse-graining, where local structure prediction is not expected, and it is more important to capture the average thermodynamic properties of the fluid.

The inclusion of angle potentials in the SAFT-γ Mie simulations slightly perturbs the local structure of the fluid, as seen from RDFs involving octane sites (Figure 4a,b) but does not improve agreement with RDFs from the atomistic reference simulations.

We also investigate the ability of the models to reproduce three-body structural correlations, which is essential to the ability of a coarse-grained model to represent the underlying atomistic model well.[83] The quantity $G^3(r,r')$, given by:

$$G^3(r,r') = \left\langle \sum_i \sum_{j \neq i,k} \sum_{k \neq i,j} (\cos(\hat{\mathbf{u}}_{ij} \cdot \hat{\mathbf{u}}_{ik}) \delta(r_{ij} - r)\delta(r_{ik} - r') \right\rangle, \quad (23)$$

where $\hat{\mathbf{u}}_{ij}$ is the unit vector between sites i and j and r_{ij} is the distance between the two sites, is a useful measure of how well a model describes three-body correlations, as described by Noid *et al.*[83] $G^3(r,r')$ is a measure of the average angle between the vectors $\hat{\mathbf{u}}_{ij}$ and $\hat{\mathbf{u}}_{ik}$, as a function of the distances between the sites. This quantity was calculated for the RRR and RAA triplets from simulations of the $x_{oct} = 0.5$ mixture, using the IBI, HFM and SAFT-γ Mie models, and also for the atomistic trajectory mapped to a coarse-grained representation. These results are shown in Figure 5 for $r' = 0.5$ nm. The IBI and HFM models both compare well to the atomistic reference in both cases. However, the HFM results are slightly less accurate; this is expected, given that HFM performs slightly worse than IBI in reproducing RDFs. These results are encouraging given that the target of both methods is to match two-body correlations. The negative peaks at around $r = 0.6$ nm indicate the exclusion of particle j from the immediate surroundings of particle k, while the positive peaks at around $r = 0.9$ nm represent the strong probability of finding particle j at a distance corresponding to the second peak on the RDF. The SAFT-γ Mie model does not represent three-body correlations well, which is not surprising given its poor representation of the site-site RDFs.

3.5 Transferability

The potentials obtained from both IBI and HFM *bottom-up* methods differ somewhat when obtained from different reference sys-
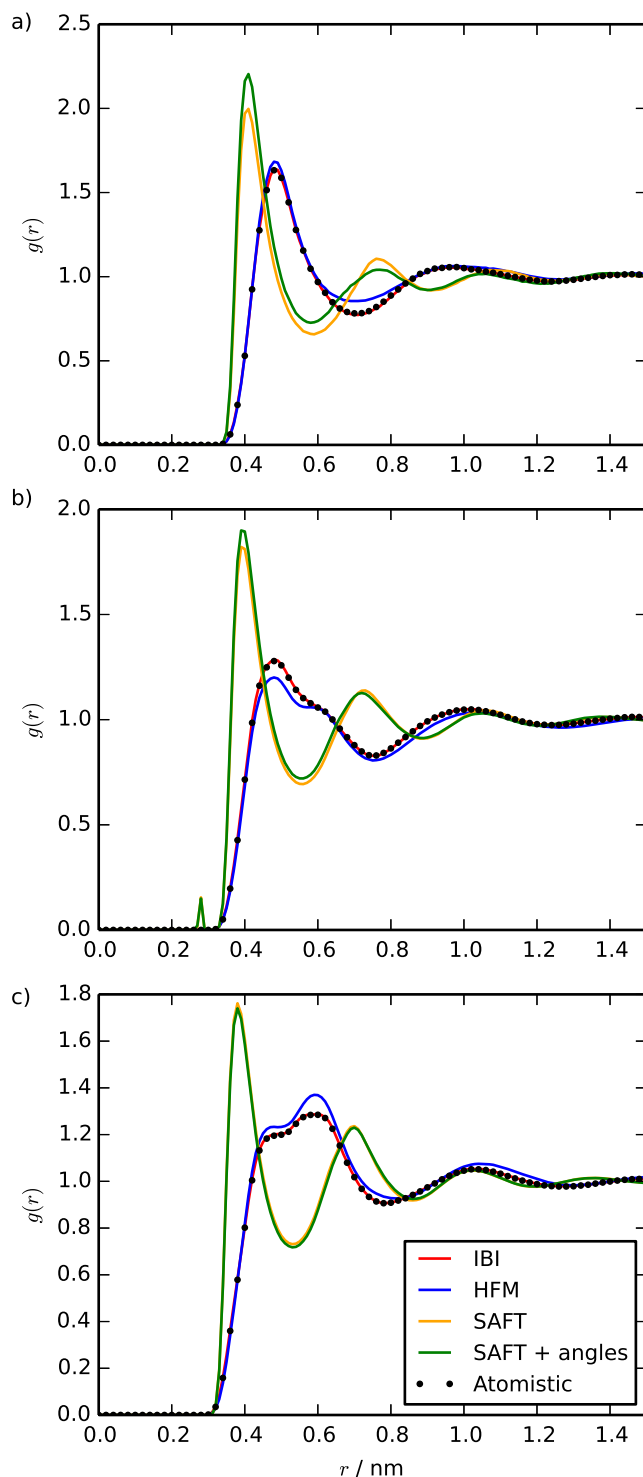

Fig. 4 Intermolecular radial distribution functions, at 298 K and 1 bar, for the $x_{oct} = 0.3$ system from atomistic reference simulations, IBI and HFM models parametrised at this concentration and the SAFT-γ Mie model, both with and without angle potentials: a) A-A, b) A-R and c) R-R interactions.

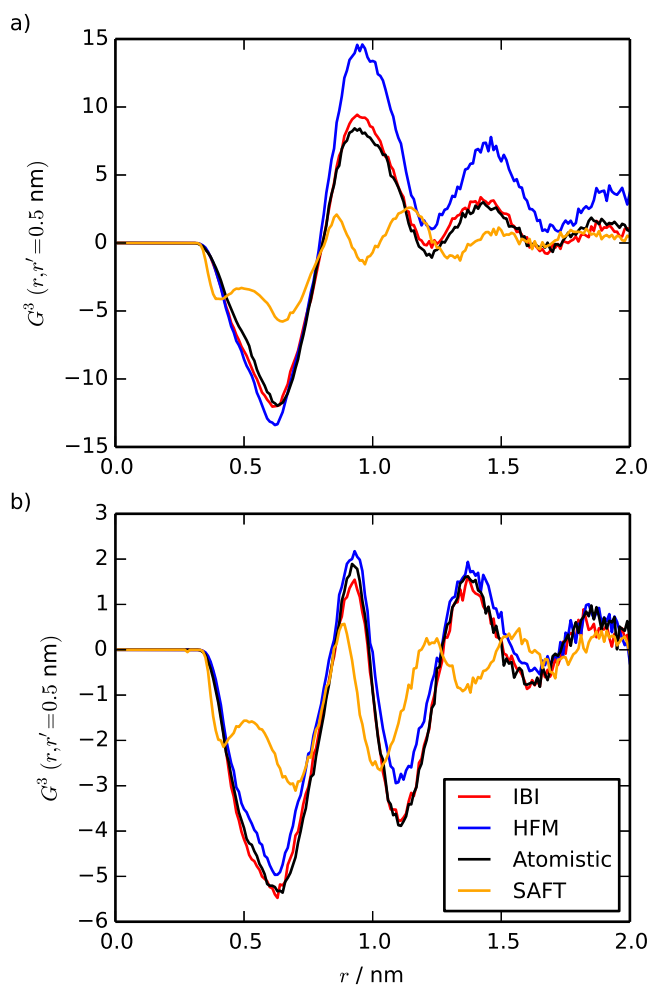**Fig. 5** Three-body correlations calculated for the $x_{oct} = 0.5$ system, for the a) RRR and b) RAA triplets, calculated using atomistic, IBI, HFM and SAFT-γ Mie models. Note that intramolecular pairs are excluded from these calculations.

tem concentrations. This is illustrated in Figure 6 for the A-A interaction using IBI and HFM. Here, particularly for the HFM case, there is considerable variation in the overall shape of the effective pair potential across the concentration range. The A-A potential varies most with concentration and there is a smaller change for other pair potentials, particularly the R-R potential (see ESI).

This immediately suggests that the models will not be particularly transferable, and this turns out to be the case. Figure 7 shows a comparison with the A-A partial RDF obtained from atomistic simulations at $x_{oct} = 0.2$, using HFM models parametrised at $x_{oct} = 0.2$ and $x_{oct} = 0.5$. The HFM results are significantly worse for the higher octane concentration. Moreover, the HFM potential parametrised at $x_{oct} = 0.5$, is unable to reproduce the correct density for any other concentration.

In contrast to the results for standard IBI, MS-IBI was successful in constructing a concentration transferable model. After the application of pressure correction during the MS-IBI process, the MS-3c and MS-4c models both gave pressures of close to 1 bar at the atomistic density for all of the reference concentrations used

in the parametrisation, as shown for MS-4c in Figure 8. Although we have not plotted the results here, the density/concentration relationship of the MS-3c model is indistinguishable from that of MS-4c. The MS-3c model reproduced all of the RDFs quite well at $x_{oct} = 0.0$, 0.5 and 1.0. However, it should be noted that, at low octane concentrations ($x_{oct} = 0.2$ and 0.3), the RDFs involving benzene were reproduced slightly better than those involving octane and this was reversed at higher octane concentrations ($x_{oct} = 0.7$ and 0.8). This is not surprising as the model works best at concentrations at which it was parametrised, and the performance gets progressively worse as the concentration moves away from the reference state points. The MS-4c model encompasses a wider concentration range for all of the interactions, and as such, the structural accuracy is better across the range. Non-bonded distributions across the concentration range for the MS-3c and MS-4c are included in the ESI.

Both single-state *bottom-up* models show poor temperature transferability when compared to the atomistic reference system. For pure octane, the densities of the coarse-grained systems diverged from the atomistic density on increasing or decreasing the temperature from 298 K, as shown in Figure 8b. The poor temperature transferability of IBI potentials for simple liquids has been shown in the past.[84] These results show that HFM suffers from exactly the same problem. The similarity of the results from the two methods likely comes from the fact that the same method was used for pressure correction in each case. The *ad hoc* nature of the linear pressure correction means that there is no guarantee of transferability to different state points.

The MS-2t model was not able to reproduce the atomistic densities across the range of temperatures any better than the IBI model. This was expected given that, during the parametrisation process, the pressures of the two coarse-grained systems converged respectively to slightly above and slightly below the target pressure of 1 bar. As discussed above, this is in contrast to the excellent thermal expansion behaviour seen for simple Mie potentials fitted via the SAFT-γ Mie EoS (Figure 3).

Non-bonded distributions for all three MS-IBI models are included in the ESI. Despite the differences between the models described above, the structural accuracy of all of the MS-IBI models is generally better than HFM, and particularly SAFT-γ Mie. It should, however, be noted that the differences between the RDFs at each state-point are relatively small, which perhaps makes the job of simultaneously matching all of them easier. It would interesting to investigate the performance of the MS-IBI method if the differences between the reference systems were more pronounced; for example, if the temperature or concentration range considered spanned one or more phase boundaries. In this case, convergence of the MS-IBI iterations may be more difficult.

3.6 Solvation free energies

The solvation free energies of octane and benzene are consistently overestimated by pressure-corrected HFM for all of the systems studied. However, as can be seen in Figure 9, there is no systematic relationship between the atomistic and HFM solvation free energies, with the difference between the two varying sig-
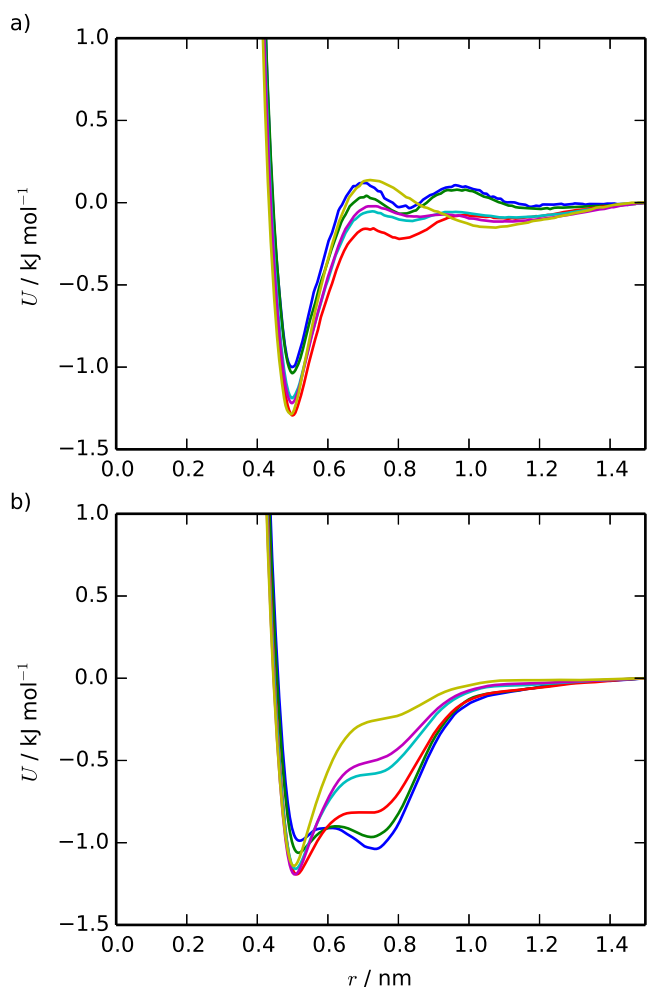
Fig. 7 Radial distribution function for the A-A interaction for simulations of $x_{oct} = 0.2$ at 298 K and 1 bar: atomistic reference, HFM parametrised for $x_{oct} = 0.2$, and HFM parametrised for $x_{oct} = 0.5$

Fig. 6 Coarse-grained intermolecular potentials for a) A-A IBI and b) A-A HFM, parametrised at 298 K. Each potential in each plot is from a different octane concentration: 20% (blue), 30% (green), 50% (red), 70% (cyan), 80% (purple) and 100% (yellow).

nificantly over the concentration range.

HFM without pressure correction performed extremely poorly, as shown in Figure 9. All of the solvation free energies from these models are very far off the atomistic values; most notably, benzene is predicted to be insoluble in pure benzene.

The difference between the pressure corrected and non-pressure corrected HFM models highlights the problem of coarse-grained models properly representing thermodynamic properties. It is known that the state-dependence of coarse-grained potentials affects the ability of coarse-grained models to reproduce the pressure, since the virial formula does not take into account the volume dependence of the potentials.[9] This has ramifications for the calculation of free energies for coarse-grained models. The incorrect representation of the pressure of the coarse-grained model leads to an incorrect representation of free energy changes (since $(\partial A/\partial V)_T = -P$); this explains the poor performance of the non-pressure corrected models. The application of pressure correction also improves the accuracy of free energy changes at a single state-point. However, because the linear pressure correction we
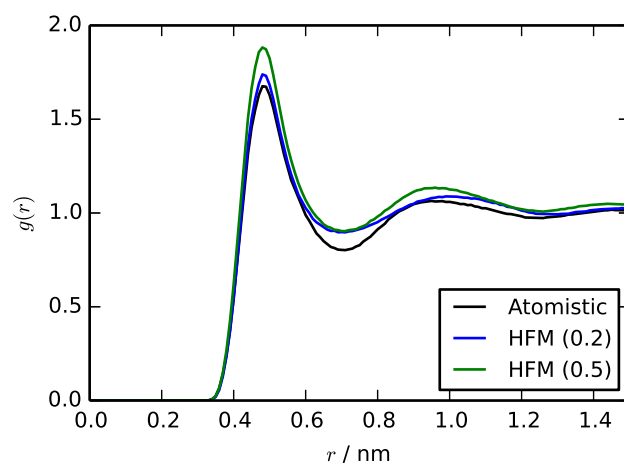
have applied does not properly address the volume dependence of the coarse-grained potentials, this is unlikely to be transferable to other state-points.

For all systems, the IBI model predicts the solvation free energy of both benzene and octane more accurately than the HFM model. This could be attributed to the way in which the pressure correction is carried out for each method. In the IBI procedure, the pressure correction is carried out in conjunction with structure matching, and so the resulting model is guaranteed to reproduce both the structure and the pressure. This is only possible due to the iterative nature of IBI; it is trivial to add extra steps to the structure matching procedure to introduce the extra constraints. For force matching, on the other hand, the pressure correction is applied after the force matching procedure, and so there is less of a guarantee that both the forces and the pressure will be correct. Matching the pressure at the same time as the forces would require either the introduction of another set of equations or terms to the force matching equations (as shown, for example, by Das and Andersen)[63] or adapting the iterative force matching method suggested by Lu *et al.* to self-consistently match the pressure.[85]

The MS-4c model shows a marked improvement over the IBI models in the calculation of solvation free energies, in terms of both representability and transferability. It was shown in Figure 8 that the MS-4c model is able to reproduce the atomistic pressure right across the concentration range; this translates to an accurate reproduction of the trend in solvation free energy across the same concentration range, as seen in Figure 9. This is in contrast to the IBI models, where a single model will not be thermodynamically transferable across the concentration range, and so accurate representation of the pressure and solvation free energy at a given concentration requires the use of a model parametrised specifically for that concentration. The necessity of using a separate coarse-grained model for each state-point impacts the ability of IBI to replicate the trend in solvation free energy across the concentration range; this is shown by the differing line-shapes
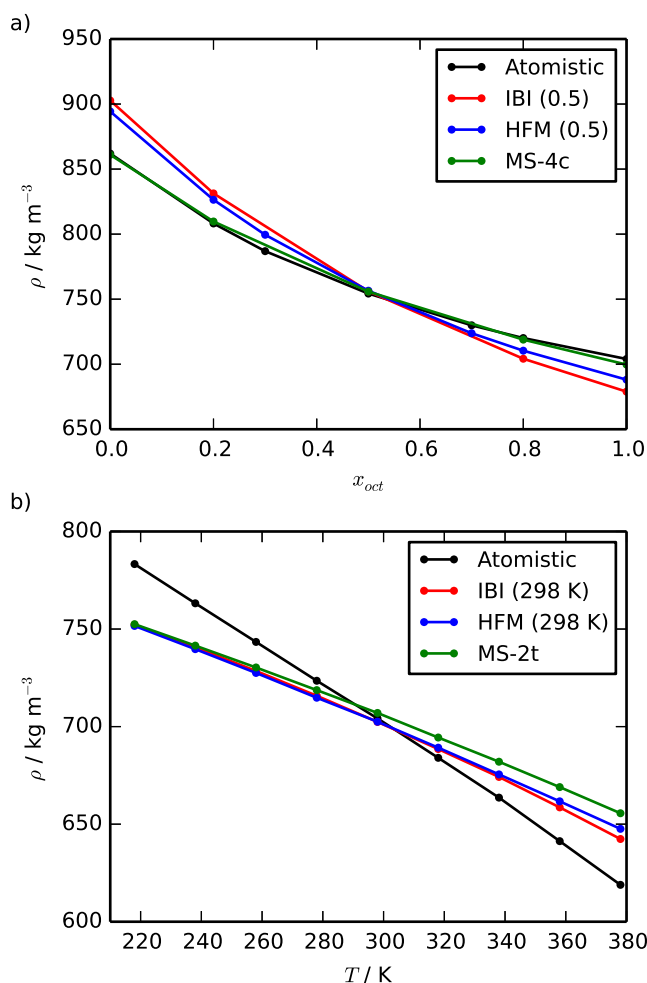
Fig. 8 Transferability of densities calculated by different coarse-grained models. The IBI and HFM models were: a) parametrised at $x_{oct} = 0.5$, 298 K and 1 bar, and b) parametrised for pure octane at 298 K and 1 bar, and run at the specified temperature.

Fig. 9 Free energies of solvation of a) octane and b) benzene as a function of solvent concentration, for atomistic, IBI, MS-IBI, HFM with pressure correction, HFM without pressure correction, and SAFT-γ Mie simulations. (The IBI and HFM *bottom-up* potentials are parametrised for each independent state point.)

produced by the IBI models in Figure 9, compared to those of the atomistic and MS-4c models.

The SAFT-γ Mie model is also able to predict solvation free energies, and their trend with respect to concentration, with fairly good accuracy. The SAFT equation of state is designed to accurately calculate free energies, so it is encouraging that a CG force field based on it performs reasonably well on such quantities. The introduction of angle potentials to the SAFT-γ Mie model does not affect the value of ΔG_{sol} within our calculated errors, despite the small changes seen in the shape of the radial distribution function in Figure 4.

4 Discussion

The Henderson uniqueness theorem[86] states that a pair potential which is able to reproduce the RDF of a simple liquid will be unique. This unique potential is the target of IBI and other structure-based coarse-graining methods. However, we know from previous studies of IBI potentials that, even if a coarse-grained model exactly matches the RDFs from an atomistic sys-
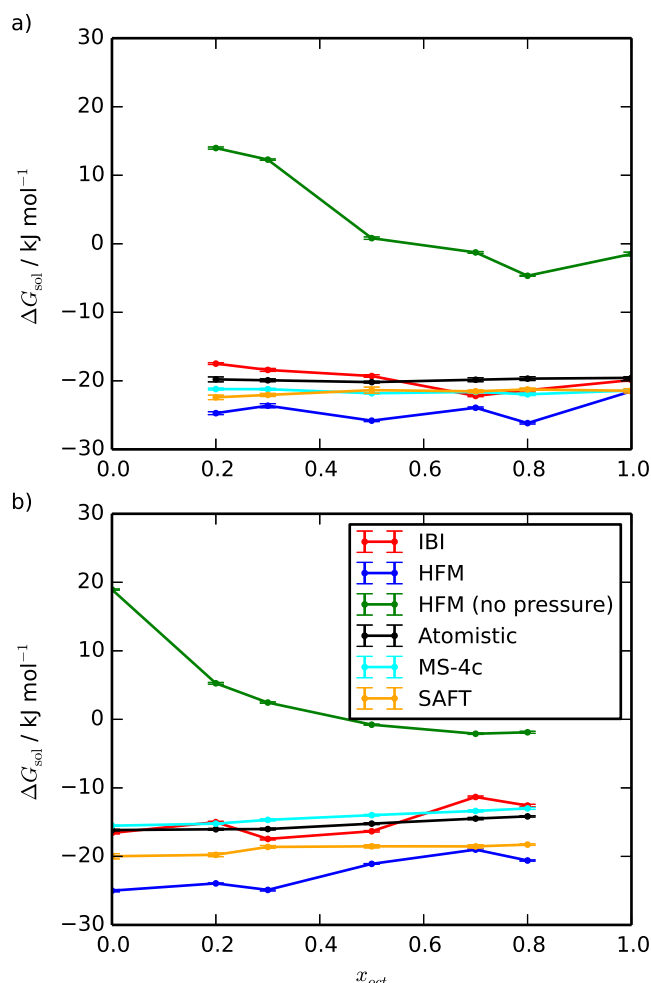
tem, this provides no guarantees that the thermodynamic properties will be reasonable.[87] Moreover, as seen in some previous work[84] potentials generated with IBI method tend to have limited transferability, both in terms of concentration and temperature (though the degree of transferability is clearly system-dependent). The form of the effective pair potential differs significantly with concentration. This seems to be exaggerated by the presence of physically undesirable oscillations in the potential as a function of distance; so that the concentration-dependent pair potential changes even at large separations.

The MS-IBI approach clearly improves on the results from IBI. In practice, MS-IBI offers a compromise where slightly worse fits to pairwise RDFs allow a better representation of some thermodynamic properties and improved transferability. However, this is at some additional computational cost in terms of fitting. Moreover, the oscillations of the effective potential, are not eliminated by this method and for pressure-consistent potentials to be produced, further pressure corrections may be required. This can

make it more difficult to achieve a single temperature transferable potential (noting that a "too high" pressure in one reference system can be balanced by a "too low" pressure in another). We also note that the burden of producing IBI (or MS-IBI) potentials increases dramatically with the number of different types of coarse-grained beads. As each pair interaction needs to be fitted, the practical application of IBI/MS-IBI for complex systems is extremely computationally expensive.

The failure of MS-IBI to produce a single temperature transferable model highlight the difficult of achieving this in a coarse-grained model. Some success has been achieved by scaling or reweighting a model developed at one temperature to other temperatures, using the MS-CG[88] and IBI[23,89] methods. The conditional reversible work method has been fairly successful at achieving a temperature transferablity, although the model has worse representability at the temperature for which it was parametrised, compared to pressure-corrected IBI.[84] Ultimately, the issue of temperature transferability in a pair potential is one that is yet to be solved, and doing so will require addressing the differences in the free-energy decomposition with temperature which come to the fore when coarse-graining.[90]

Given the excellent structural predictions from IBI, it is interesting to ask whether there are other related approaches that could improve the basic method. Of interest here, is the previous work of Lyubartsev *et al.*,[91] who showed that the coarse-graining of water via Newton inversion could be carried out in the liquid-vapour two-phase region. Here, matching of the RDF leads to pair potentials that seem to give a better representation of pressure than those arising from IBI of bulk water. Motivated by this work, we used MS-IBI in the vapour and liquid phases of octane and found the resultant potentials do give good pressures; however, the model was no more temperature transferable than the other models presented in this paper.

The HFM used in this work does remarkably well in terms of prediction of local structure, noting that it is not fitted to reproduce this. The simple pressure correction term that we introduce in the current paper does not noticeably change local structure but does allow the pressure to be corrected by small changes to the effective pair potential, and thereby allows HFM to work under conditions of const-NpT.

Unfortunately, for the octane-benzene mixture the effective pair potentials produced with HFM change even more than IBI potentials with concentration. So transferability for these potentials is rather poor. (Noting that there is no theoretical basis to expect coarse-grained pair potentials to be similar across state points.) One possible solution is to include three-body terms. For simple systems, this is known to improve representability.[92,93] It may also allow a coarse-grained model to react better to its environment, for example in the modelling of a phase-separated liquid mixture.[94] However, it is not guaranteed that three-body terms alone would address all the causes of poor transferability in coarse-grained models; specifically, the multi-body PMF for the system contains many contributions that are state-point dependent, which it may not be possible to match using only configuration-dependent potentials.[20,95]

Chemically transferable models, whether between different concentrations or between similar chemical systems, are crucial, as they reduce the time otherwise spent parametrising models for each state point. Models developed by the conditional reversible work method have been shown to be transferable between different alkane chain lengths.[96] However, as the authors note, this method is not necessarily applicable to more complex systems. The extended ensemble approach of Mullinax and Noid,[97] in which the coarse-grained potential is parametrised for an ensemble of systems simultaneously, allows for concentration transferable models, although at the cost of some representability compared to models parametrised for a single system. This approach was extended by Dunn and Noid[98] to include volume potentials, yielding a set of related models which, together, can give both temperature and concentration transferability.

The linear pressure correction which has been applied in this work is very effective at correcting the coarse-grained pressure for a given state-point, without requiring the inclusion of any other parameters in the coarse-grained force field. However, it does not do so in a transferable way; in fact, it has been shown by Wang *et al.*[99] that correcting the pressure in this way means that the compressibility of the model will no longer be correct. The reason for this is that the linear correction does not take into account the underlying issue with the representation of pressure in coarse-grained models; the effective pair potentials generated by IBI and HFM are volume-dependent, and so the virial formula for calculating pressure is not valid.[9] The volume potentials first suggested by Das and Anderson[63], on the other hand, are able to simultaneously represent pressure and compressibility,[100] because they explicitly take into account the volume-dependence of coarse-grained potentials. This approach has recently been used to construct a temperature transferable coarse-grained model,[101] although this is, of course, at the expense of adding extra parameters to the model, and therefore slowing down the coarse-grained simulations.

The SAFT-γ Mie EoS is an intriguing approach to *top-down* coarse-graining. As an EoS, SAFT-γ Mie is remarkably accurate when fitted to produce a wide range of experimental data. The possibility of being able to fit Mie potentials to reproduce, for example, vapour-liquid coexistence data over a range of temperatures guarantees that optimised effective pair potentials will be produced that are transferable in terms of thermodynamic free energies. However, there are problems with SAFT-γ Mie potentials in terms of local structure prediction. These problems have their origin in the use of tangential spheres and the lack of angle-dependent terms. Both are quite serious practical problems. The former leads to a local structure that is fundamentally different to that seen in conventional coarse-grained models. In some cases, such as in the recent work on chromonics by Potter and co-workers,[17] where a SAFT-γ Mie EoS is used to parametrise molecular fragments, the local bead packing arrangement leads to an unphysical stacking of molecules, promotes phase separation and therefore limits both representability and transferability within a molecular dynamics model. Within the SAFT framework, the use of shape factors[102] is an interesting suggestion that may go some way to solving this problem. However, this would be difficult to implement for systems with multiple bead types. Al-

ternative *top-down* approaches may also be effective; for example, a recent study by An *et al.* presents a coarse-grained model for alkane chains parametrised using a particle swarm optimisation strategy. This model is both transferable, and exhibits good structural accuracy. [103]

In the current work, the addition of angle terms to the molecular dynamics simulations made only a small difference to the SAFT-γ Mie results. In this case, there did not appear to be a particularly strong coupling between these terms and the optimal values of the nonbonded parameters ε, σ, λ_r and λ_a. For other systems, we might expect this link to be more significant. For comparison, researchers have found that in DPD simulations there is a strong link between the calculated values of various thermodynamic quantities, and the strength of the connecting springs used to link beads. [104,105] So for example, in DPD, it is possible to fit A_{ij} parameters for a bead by calculating changes in free energy for insertion of particles; hence infinite dilution activity coefficients are very valuable in DPD parametrisation. [106] However, the local environment sampled by a bead is altered significantly by the bond and angle terms within a DPD model; and this can be quite problematic. In principle, it is possible to envisage derivation of additional 3-body and 4-body terms within a SAFT framework (current SAFT theories are based on first-order Wertheim perturbation theory). However, a derivation of the corresponding equations, and a simplified version of these that can be added to the existing SAFT equations, has so far not been achieved due to the complex nature of the equations that arise.

It is worth noting that in the current work we have used standard combining rules for benzene-octane cross-interactions. This is superficially very attractive because the parametrisation task for systems with many beads becomes far less onerous when all the cross-interaction terms do not need to be fitted. Unfortunately, for many systems the combining rules do not work as well. [107] However, simple improvements to the fitting of thermodynamic data within SAFT-γ Mie can be made by allowing the k_{ij} parameter to vary from zero. [108]

A further interesting comparison between the *bottom-up* and *top-down* approaches is the shape of the potentials they produce. As shown in Figure 6, the *bottom-up* methods produce a wide variety of potential shapes, which do not correspond to a common functional form. In principle, the use of numerical or spline potentials allows for greater flexibility when trying to match the reference properties. In practice, however, it can result in overfitting the model to a particular state point. The reason for the irregular bumps present in many of these potentials is that they are effective pair potentials, in which any multi-body contributions resulting from the coarse graining of the system are included only in an averaged way. This will only be applicable to the state point at which the model was parametrised since the local environment of a given bead will vary depending on the temperature and concentration. SAFT-γ Mie models, on the other hand, are based entirely on Mie potentials, with a distinct functional form described in Equation 12. Because of this well-defined shape, there is less danger of overfitting; therefore, they are likely to have much better transferability than IBI or HFM models.

Finally, given the difficulties in achieving the two key chemi-

cally desirable attributes (i.e. local structure and thermodynamics) within a single coarse-grained model, it is appropriate to ask the question as to whether it is possible to have this level of representability, together with transferability to other state points. We would strongly argue that, in principle, it is. In one sense, all classical models can be thought of as existing on a continuum scale of complexity: atomistic models are largely successful because typical force fields have achieved a reasonably high degree of representability and transferability. Yet we know that if, for example, a TIP4P water molecule is transferred from bulk water into the gas phase (an environment with a different density) or transferred to the surface of a protein (an environment with a dielectric constant) then the TIP4P water is not as good a model as it is for bulk water. The way around this transferability problem is partly being tackled by polarizable models, such as AMOEBA; [109] i.e. models that can respond to environmental changes. For coarse-grained models it is desirable to do the same, without the obvious but prohibitively expensive, addition of full three-body forces to a method such as HFM. Recent work provides some encouragement that this can be achieved due to the improvements of the transferability in DPD models via addition of a local density-dependent term (MDPD). [110] Crucially, the computational cost of this local density-dependent term scales with system size like a simple pair potential. A similar approach has been applied to transferable *bottom-up* coarse-grained models of a range of systems, including liquid-liquid and liquid-vapour equilibria. This includes interactions which are transferable between bulk liquids and liquid-liquid interfaces, which is a notable improvement in chemical transferability. [39,65,111–113]

5 Conclusions

In this paper, we have compared the accuracy and transferability of coarse-grained models parametrised using *top-down* (SAFT-γ Mie) and *bottom-up* (IBI, HFM and MS-IBI) methods. Both approaches were found to have distinct advantages and disadvantages.

In terms of structural accuracy, IBI was found to be superior to both HFM and SAFT-γ Mie. MS-IBI models were almost as accurate, although the use of multiple reference systems meant the loss of some accuracy for individual state points. HFM models were able to reproduce the structure of the systems studied fairly well, while SAFT models were not able to give an accurate picture of the local structure of any of the systems. Unfortunately, even for this simple system, the effective pair potentials derived in each process vary considerably between state points, limiting transferability.

In terms of thermodynamics, although neither *bottom-up* method was able to reproduce exactly the solvation or mixing free energies of the atomistic system, the accuracy was good enough that the correct phase behaviour was observed. Pressure correction was found to be crucial for the reproduction of solvation free energies, confirming that matching structure or forces alone does not guarantee thermodynamic consistency when moving to a coarse-grained representation of a system. Models derived from SAFT-γ Mie were found to be thermodynamically transferable across a range of temperatures and concentrations.

MS-IBI models improve the transferability of the IBI method, although they are not guaranteed to be a complete solution. The failure of MS-IBI to produce a temperature transferable model of octane highlights a fundamental difficulty with *bottom-up* coarse graining. Removing degrees of freedom will always reduce the entropy of the system, so in order to match the free energy, the enthalpy/entropy balance must be shifted. Since the entropic contribution to the free energy is temperature dependent (including the contribution to the entropy from degrees of freedom that have been removed), the overall free energy of the system will not scale correctly with temperature, and the force field will not be completely transferable. SAFT models tend to be considerably better in terms of thermodynamic transferability, due to fitting over a range of state points. Unfortunately, this is at the expense of very poor structural accuracy.

Finally, we discussed in detail, possible ways forward for coarse-graining, which may eventually address the problems of structure prediction, correct thermodynamics and improved transferability.

Acknowledgements

Disclosure statement

There are no conflicts of interest to report.

Supplemental data

Supplemental data for this article are available.

References

1 A. Gooneie, S. Schuschnigg and C. Holzer, *Polymers*, 2017, **9**, 16.

2 J. L. Bouvard, D. K. Ward, D. Hossain, S. Nouranian, E. B. Marin and M. F. Horstemeyer, *J. Eng. Mater. Technol*, 2009, **131**, 041206–041206–15.

3 A. Warshel, *Angew. Chem. Int. Ed.*, 2014, **53**, 10020–10031.

4 S. F. Sousa, A. J. Ribeiro, R. P. Neves, N. F. Brás, N. M. Cerqueira, P. A. Fernandes and M. J. Ramos, *Wiley Interdiscip. Rev.: Comput. Mol. Sci.Science*, 2017, **7**, e1281.

5 C. Krekeler, A. Agarwal, C. Junghans, M. Praprotnik and L. Delle Site, *J. Chem. Phys.*, 2018, **149**, 024104.

6 R. Fiorentini, K. Kremer, R. Potestio and A. C. Fogarty, *J. Chem. Phys.*, 2017, **146**, 244113.

7 R. Potestio, C. Peter and K. Kremer, *Entropy*, 2014, **16**, 4199–4245.

8 A. J. Rzepiela, M. Louhivuori, C. Peter and S. J. Marrink, *Phys. Chem. Chem. Phys.*, 2011, **13**, 10437–10448.

9 J. W. Wagner, J. F. Dama, A. E. P. Durumeric and G. A. Voth, *J. Chem. Phys.*, 2016, **145**, 044108.

10 E. Brini, E. A. Algaer, P. Ganguly, C. Li, F. Rodríguez-Ropero and N. F. van der Vegt, *Soft Matter*, 2013, **9**, 2108–2119.

11 S. J. Marrink, H. J. Risselada, S. Yefimov, D. P. Tieleman and A. H. de Vries, *J. Phys. Chem. B*, 2007, **111**, 7812–7824.

12 S. J. Marrink and D. P. Tieleman, *Chem. Soc. Rev.*, 2013, **42**, 6801–6822.

13 C. Peter and K. Kremer, *Soft Matter*, 2009, **5**, 4357.

14 C. Peter and K. Kremer, *Faraday Discuss.*, 2010, **144**, 9–24.

15 A. A. Louis, *J. Phys.: Condens. Matter*, 2002, **14**, 9187.

16 M. E. Johnson, T. Head-Gordon and A. A. Louis, *J. Chem. Phys.*, 2007, **126**, 144509.

17 T. D. Potter, J. Tasche, E. L. Barrett, M. Walker and M. R. Wilson, *Liq. Cryst.*, 2017, **44**, 1979–1989.

18 M. Walker, A. J. Masters and M. R. Wilson, *Phys. Chem. Chem. Phys.*, 2014, **16**, 23074–23081.

19 E. C. Allen and G. C. Rutledge, *J. Chem. Phys.*, 2009, **130**, 034904.

20 N. J. H. Dunn, T. T. Foley and W. G. Noid, *Acc. Chem. Res.*, 2016, **49**, 2832–2840.

21 A. Soper, *Chem. Phys.*, 1996, **202**, 295–306.

22 P. Carbone, H. A. K. Varzaneh, X. Chen and F. Müller-Plathe, *J. Chem. Phys.*, 2008, **128**, 064904.

23 H.-J. Qian, P. Carbone, X. Chen, H. A. Karimi-Varzaneh, C. C. Liew and F. Müller-Plathe, *Macromolecules*, 2008, **41**, 9919–9929.

24 K. Prasitnok and M. R. Wilson, *Phys. Chem. Chem. Phys.*, 2013, **15**, 17093–17104.

25 L. Saiz and M. L. Klein, *Account. Chem. Res.*, 2002, **35**, 482–489.

26 S. J. Marrink, A. H. de Vries and D. P. Tieleman, *Biochim. Biophys. Acta, Biomembr.*, 2009, **1788**, 149–168.

27 A. Catte, M. R. Wilson, M. Walker and V. S. Oganesyan, *Soft Matter*, 2018, **14**, 2796–2807.

28 P. Setny and M. Zacharias, *Nucleic Acids Res.*, 2011, **39**, 9118–9129.

29 R. Pool and P. G. Bolhuis, *J. Phys. Chem. B*, 2005, **109**, 6650–6657.

30 E. N. Brodskaya, *Colloid J.*, 2012, **74**, 154–171.

31 W. Shinoda, R. DeVane and M. L. Klein, *Mol. Sim.*, 2007, **33**, 27–36.

32 X. He, W. Shinoda, R. DeVane, K. L. Anderson and M. L. Klein, *Chem. Phys. Lett.*, 2010, **487**, 71–76.

33 M. Walker and M. R. Wilson, *Soft Matter*, 2016, **12**, 8588–8594.

34 R. D. Groot and T. J. Madden, *J. Chem. Phys.*, 1998, **108**, 8713–8724.

35 A. A. Gavrilov, Y. V. Kudryavtsev and A. V. Chertovich, *J. Chem. Phys.*, 2013, **139**, 224901.

36 J. S. Lintuvuori and M. R. Wilson, *Phys. Chem. Chem. Phys.*, 2009, **11**, 2116–2125.

37 C. Zannoni, *J. Mater. Chem.*, 2001, **11**, 2637–2646.

38 M. Walker and M. R. Wilson, *Soft Matter*, 2016, **12**, 8876–8883.

39 J. W. Wagner, T. Dannenhoffer-Lafage, J. Jin and G. A. Voth, *J. Chem. Phys.*, 2017, **147**, 044113.

40 J. M. Wang, R. M. Wolf, J. W. Caldwell, P. A. Kollman and D. A. Case, *J. Comp. Chem.*, 2004, **25**, 1157–1174.

41 N. J. Boyd and M. R. Wilson, *Phys. Chem. Chem. Phys.*, 2015, **17**, 24851–24865.

42 N. J. Boyd and M. R. Wilson, *Phys. Chem. Chem. Phys.*, 2018, **20**, 1485–1496.

43 S. Pronk, S. Páll, R. Schulz, P. Larsson, P. Bjelkmar, R. Apostolov, M. R. Shirts, J. C. Smith, P. M. Kasson, D. van der Spoel, B. Hess and E. Lindahl, *Bioinformatics*, 2013, **29**, 845–854.

44 S. Nosé, *J. Chem. Phys.*, 1984, **81**, 511–519.

45 W. G. Hoover, *Phys. Rev. A*, 1985, **31**, 1695–1697.

46 M. Parrinello and A. Rahman, *J. Appl. Phys.*, 1981, **52**, 7182–7190.

47 U. Essmann, L. Perera, M. L. Berkowitz, T. Darden, H. Lee and L. G. Pedersen, *J. Chem. Phys.*, 1995, **103**, 8577–8593.

48 B. Hess, H. Bekker, H. J. C. Berendsen and J. G. E. M. Fraaije, *J. Comput. Chem.*, 1997, **18**, 1463–1472.

49 V. Rühle, C. Junghans, A. Lukyanov, K. Kremer and D. Andrienko, *J. Chem. Theory Comput.*, 2009, **5**, 3211–3223.

50 V. Rühle and C. Junghans, *Macromol. Theory Simul.*, 2011, **20**, 472–477.

51 S. Y. Mashayak, M. N. Jochum, K. Koschke, N. R. Aluru, V. Rühle and C. Junghans, *PLOS ONE*, 2015, **10**, e0131754.

52 D. Reith, M. Pütz and F. Müller-Plathe, *J. Comput. Chem.*, 2003, **24**, 1624–1636.

53 T. C. Moore, C. R. Iacovella and C. McCabe, *J. Chem. Phys.*, 2014, **140**, 224104.

54 T. C. Moore, C. R. Iacovella, R. Hartkamp, A. L. Bunge and C. McCabe, *J. Phys. Chem. B*, 2016, **120**, 9944–9958.

55 S. Izvekov and G. A. Voth, *J. Phys. Chem. B*, 2005, **109**, 2469–2473.

56 S. Izvekov and G. A. Voth, *J. Chem. Phys.*, 2005, **123**, 134105.

57 W. G. Noid, J. W. Chu, G. S. Ayton, V. Krishna, S. Izvekov, G. A. Voth, A. Das and H. C. Andersen, *J. Chem. Phys.*, 2008, **128**, 244114.

58 L. Lu, S. Izvekov, A. Das, H. C. Andersen and G. A. Voth, *J. Chem. Theory Comput.*, 2010, **6**, 954–965.

59 P. Liu, S. Izvekov and G. A. Voth, *J. Phys. Chem. B*, 2007, **111**, 11566–11575.

60 A. Das, L. Lu, H. C. Andersen and G. A. Voth, *J. Chem. Phys.*, 2012, **136**, 194115.

61 Y. Wang, S. Izvekov, T. Yan and G. A. Voth, *J. Phys. Chem. B*, 2006, **110**, 3564–3575.

62 L. Lu and G. A. Voth, *J. Phys. Chem. B*, 2009, **113**, 1501–1510.

63 A. Das and H. C. Andersen, *J. Chem. Phys.*, 2010, **132**, 164106.

64 N. J. H. Dunn and W. G. Noid, *J. Chem. Phys.*, 2016, **144**, 204124.

65 M. R. DeLyser and W. G. Noid, *J. Chem. Phys.*, 2017, **147**, 134111.

66 E. A. Müller and G. Jackson, *Annu. Rev. Chem. Biomol. Eng.*, 2014, **5**, 405–427.

67 T. Lafitte, A. Apostolakou, C. Avendaño, A. Galindo, C. S. Adjiman, E. A. Müller and G. Jackson, *J. Chem. Phys.*, 2013, **139**, 154504.

68 J. A. Barker and D. Henderson, *Reviews of Modern Physics*, 1976, **48**, 587.

69 M. Wertheim, *J. Stat. Phys.*, 1984, **35**, 19–34.

70 M. Wertheim, *J. Stat. Phys.*, 1984, **35**, 35–47.

71 M. Wertheim, *J. Stat. Phys.*, 1986, **42**, 459–476.

72 M. Wertheim, *J. Stat. Phys.*, 1986, **42**, 477–492.

73 M. S. Wertheim, *J. Chem. Phys.*, 1986, **85**, 2929–2936.

74 M. S. Wertheim, *J. Chem. Phys.*, 1987, **87**, 7323–7331.

75 C. Avendaño, T. Lafitte, A. Galindo, C. S. Adjiman, G. Jackson and E. A. Müller, *J. Phys. Chem. B*, 2011, **115**, 11154–11169.

76 C. Avendaño, T. Lafitte, C. S. Adjiman, A. Galindo, E. A. Müller and G. Jackson, *J. Phys. Chem. B*, 2013, **117**, 2717–2733.

77 V. Papaioannou, T. Lafitte, C. Avendaño, C. S. Adjiman, G. Jackson, E. A. Müller and A. Galindo, *J. Chem. Phys.*, 2014, **140**, 054107.

78 T. Lafitte, C. Avendaño, V. Papaioannou, A. Galindo, C. S. Adjiman, G. Jackson and E. A. Müller, *Mol. Phys.*, 2012, **110**, 1189–1203.

79 A. Mejía, C. Herdes and E. A. Müller, *Ind. Eng. Chem. Res.*, 2014, **53**, 4131–4141.

80 C. H. Bennett, *J. Comput. Phys.*, 1976, **22**, 245–268.

81 L. Morávková, Z. Wagner and J. Linek, *J. Chem. Thermodyn.*, 2008, **40**, 607–617.

82 J. H. Dymond and K. J. Young, *Int. J. Thermophys.*, 1981, **2**, 237–247.

83 W. G. Noid, J.-W. Chu, G. S. Ayton and G. A. Voth, *J. Phys. Chem. B*, 2007, **111**, 4116–4127.

84 E. Brini, V. Marcon and N. F. A. van der Vegt, *Phys. Chem. Chem. Phys.*, 2011, **13**, 10468.

85 L. Lu, J. F. Dama and G. A. Voth, *J. Chem. Phys.*, 2013, **139**, 121906.

86 R. L. Henderson, *Phys. Lett. A*, 1974, **49**, 197–198.

87 P. Ganguly, D. Mukherji, C. Junghans and N. F. A. van der Vegt, *J. Chem. Theory Comput.*, 2012, **8**, 1802–1807.

88 V. Krishna, W. G. Noid and G. A. Voth, *J. Chem. Phys.*, 2009, **131**, 024103–024103–12.

89 K. Farah, A. C. Fogarty, M. C. Bãűhm and F. Mãijller-Plathe, *Phys. Chem. Chem. Phys.*, 2011, **13**, 2894–2902.

90 L. Lu and G. A. Voth, *J. Chem. Phys.*, 2011, **134**, 224107–224107–10.

91 A. Lyubartsev, A. Mirzoev, L. Chen and A. Laaksonen, *Faraday Discuss.*, 2010, **144**, 43–56.

92 L. Larini, L. Lu and G. A. Voth, *J. Chem. Phys.*, 2010, **132**, 164107.

93 A. Das and H. C. Andersen, *J. Chem. Phys.*, 2012, **136**, 194114.

94 J. F. Dama, J. Jin and G. A. Voth, *J. Chem. Theory Comput.*, 2017, **13**, 1010–1022.

95 W. G. Noid, *J. Chem. Phys.*, 2013, **139**, 090901.

96 E. Brini and N. F. A. van der Vegt, *J. Chem. Phys.*, 2012, **137**, 154113.

97 J. W. Mullinax and W. G. Noid, *J. Chem. Phys.*, 2009, **131**, 104110.

98 N. J. H. Dunn and W. G. Noid, *J. Chem. Phys.*, 2016, **144**, 204124.

99 H. Wang, C. Junghans and K. Kremer, *Eur. Phys. J. E*, 2009, **28**, 221–229.

100 N. J. H. Dunn and W. G. Noid, *J. Chem. Phys.*, 2015, **143**, 243148.

101 D. Rosenberger and N. F. A. v. d. Vegt, *Phys. Chem. Chem. Phys.*, 2018, **20**, 6617–6628.

102 N. F. Carnahan and E. A. Müller, *Phys. Chem. Chem. Phys.*, 2006, **8**, 2619–2623.

103 Y. An, K. K. Bejagam and S. A. Deshmukh, *J. Phys. Chem. B*, 2018, **122**, 7143–7153.

104 A. G. Goicochea, M. Romero-Bastida and R. López-Rendón, *Mol. Phys.*, 2007, **105**, 2375–2381.

105 E. Deguillard, N. Pannacci, B. Creton and B. Rousseau, *J. Chem. Phys.*, 2013, **138**, 144102.

106 A. Vishnyakov, M.-T. Lee and A. V. Neimark, *J. Phys. Chem. Lett.*, 2013, **4**, 797–802.

107 E. F. Sabattié, J. Tasche, M. R. Wilson, M. W. Skoda, A. Hughes, T. Lindner and R. L. Thompson, *Soft Matter*, 2017, **13**, 3580–3591.

108 J. Tasche, *PhD thesis*, Durham University, 2018.

109 P. Ren and J. W. Ponder, *J. Phys. Chem. B*, 2003, **107**, 5933–5947.

110 P. Warren, *Phys. Rev. E*, 2003, **68**, 066702.

111 T. Sanyal and M. S. Shell, *J. Chem. Phys.*, 2016, **145**, 034109.

112 T. Sanyal and M. S. Shell, *J. Phys. Chem. B*, 2018, **122**, 5878–5693.

113 J. Jin and G. A. Voth, *J. Chem. Theory Comput.*, 2018, **14**, 2180–2197.

Table of Contents Figure
Assessing the performance of top-down and bottom-up
coarse-graining approaches.